





# Graphene Deposited on Glass Fiber Using a Non-Thermal Plasma System

Paulo V. R. Gomes, Rafael N. Bonifacio, Barbara P. G. Silva, João C. Ferreira, Rodrigo F. B. de Souza , Larissa Otubo , Dolores R. R. Lazar  and Almir O. Neto 

Instituto de Pesquisas Energéticas e Nucleares, IPEN/CNEN-SP, Av. Prof. Lineu Prestes, 2242 Cidade Universitária, São Paulo CEP 05508-000, SP, Brazil; pvrqvictor@gmail.com (P.V.R.G.); rafaelnbonifacio@hotmail.com (R.N.B.); barbara.pe@gmail.com (B.P.G.S.); jcferrei@ipen.br (J.C.F.); souza.rfb@gmail.com (R.F.B.d.S.); lotubo@usp.br (L.O.); drlazar@usp.br (D.R.R.L.)

\* Correspondence: aolivei@usp.br

**Abstract:** This study reports a bottom-up approach for the conversion of cyclohexane into graphene nanoflakes, which were then deposited onto fiberglass using a non-thermal generator. The composite was characterized using transmission electron microscopy, which revealed the formation of stacked few-layer graphene with a partially disordered structure and a d-spacing of 0.358 nm between the layers. X-ray diffraction confirmed the observations from the TEM images. SEM images showed the agglomeration of carbonaceous material onto the fiberglass, which experienced some delamination due to the synthesis method. Raman spectroscopy indicated that the obtained graphene exhibited a predominance of defects in its structure. Additionally, atomic force microscopy (AFM) analyses revealed the formation of graphene layers with varying levels of porosity.

**Keywords:** graphene bottom-up; non-thermal plasma synthesis; hydrocarbon to graphene



**Citation:** Gomes, P.V.R.; Bonifacio, R.N.; Silva, B.P.G.; Ferreira, J.C.; de Souza, R.F.B.; Otubo, L.; Lazar, D.R.R.; Neto, A.O. Graphene Deposited on Glass Fiber Using a Non-Thermal Plasma System. *Eng* **2023**, *4*, 2100–2109. <https://doi.org/10.3390/eng4030119>

Academic Editors: Leszek Adam Dobrzański, Jingwei Zhao, Christof Sommitsch, Sabu Thomas, Lech Bolesław Dobrzański, Emilia Wołowicz-Korecka, Borut Kosec, Jorge Roberto Vargas Garcia and Gilmar Ferreira Batalha

Received: 12 July 2023

Revised: 24 July 2023

Accepted: 4 August 2023

Published: 9 August 2023



**Copyright:** © 2023 by the authors. Licensee MDPI, Basel, Switzerland. This article is an open access article distributed under the terms and conditions of the Creative Commons Attribution (CC BY) license (<https://creativecommons.org/licenses/by/4.0/>).

## 1. Introduction

Graphene is a two-dimensional nanostructured material with intrinsic properties that show promising performance in various applications, including electronics, renewable energy, medicine, mechanical enforcement, and others. Since its experimental demonstration, graphene has garnered global attention from researchers due to its mechanical, structural, thermal, and electrical properties, which make it highly attractive for engineering applications. The inherent properties of graphene have been explored in various fields, including flexible transparent circuits, electronic and optoelectronic device construction, chemical sensors, and energy storage [1–3].

Over the past two decades, numerous carbon-based materials have been referred to as graphene, expanding upon its initial definition as “a monolayer of sp<sup>2</sup>-carbon atoms” [1]. According to Zhu [2], graphene has now become a generic term encompassing a wide range of carbon-based few-layer materials with distinct structures, morphologies, and sometimes even chemical compositions, heavily influenced by the preparation method.

There are two primary methods for manufacturing graphene: a top-down approach and a bottom-up approach, each with its own limitations and advantages. Antonova et al. [1] discuss the bottom-up approach, which involves growing high-quality two-dimensional carbon layers through chemical vapor deposition or epitaxial growth on SiC substrates. This method allows for precise control over thickness by utilizing various substrate catalysts and growth parameters [4].

Among the various possible substrates is fiberglass, which finds extensive applications in engineering. The deposition of graphene onto fiberglass has emerged as a promising research area, leveraging the unique properties of both materials. Graphene, with its hexagonal arrangement of carbon atoms, exhibits high electrical conductivity, exceptional mechanical strength, and a large surface area, making it an exceptional material for diverse

technological applications [5]. On the other hand, synthetic fiberglass is known for its mechanical strength, lightweight nature, and durability, making it extensively utilized in sectors such as the construction, automotive, and aerospace industries [6].

Combining graphene with fiberglass could significantly enhance the mechanical properties of the resulting composite. Graphene possesses exceptionally high tensile strength, augmenting the strength and stiffness of fiberglass and rendering it more suitable for lightweight yet robust material applications [6]. Additionally, the incorporation of graphene could improve the fatigue resistance of fiberglass, extending its lifespan under repetitive stress conditions. Research groups are developing graphene coatings for glass fiber shielding, and boosting electrical, thermal, and mechanical properties [7,8].

However, these coating techniques suffer from solvents that can remove the graphene layer from the material of interest. There are techniques in which graphene is deposited directly onto the fiber, such as laser annealing, which allows for the creation of rGO (reduced graphene oxide) films on a substrate, further enhancing the mechanical capabilities of the fiber [9,10].

In plasma applications, small graphene flakes with few layers can be produced without the use of substrates, employing a fast and controlled synthesis process. Plasma synthesis involves the decomposition of a carbon source, with carbon particle fragments formed within the gas phase of the plasma stream [3,11].

Another advantage of depositing graphene onto fiberglass lies in its electrical properties. Graphene serves as an excellent conductor of electricity, facilitating the development of conductive composites when combined with fiberglass, which is an electrical insulator. This combination holds particular interest in applications within the realm of flexible electronics and sensory devices, where fiberglass and graphene can play pivotal roles in the transmission of electrical signals. This work presents a novel, simple, cost-effective, rapid, and scalable method of depositing graphene onto fiberglass using a non-thermal plasma system.

## 2. Experimental

The graphene deposition on glass fiber was performed using a non-thermal plasma generator [12] coupled to a reaction vessel, where an arc is created (see Figure 1). In this reactor, cyclohexane (Aldrich, St. Louis, MO, USA) and Fiberglass–E-glass (Casa da Resina, Belo Horizonte, Brazil) with a boron content greater than 6% were used as the input starting materials. The composition of the fiberglass includes approximately 54% SiO<sub>2</sub>, 14% Al<sub>2</sub>O<sub>3</sub>, 6% B<sub>2</sub>O<sub>3</sub>, 22% CaO, and trace amounts of MgO, K<sub>2</sub>O, Na<sub>2</sub>O, Fe<sub>2</sub>O<sub>3</sub>, and F<sub>2</sub>, all in quantities less than 1%. In this vessel, a 60 kV arc was applied with a flow of N<sub>2(g)</sub> between a 316L steel electrode and another one made of mineral graphite until all the liquid evaporated. The fiberglass was positioned between the two electrodes. Subsequently, the produced material was washed with water and alcohol and then dried for 30 min in an oven at 180 °C. As a comparison, a sample without fiberglass was also prepared.

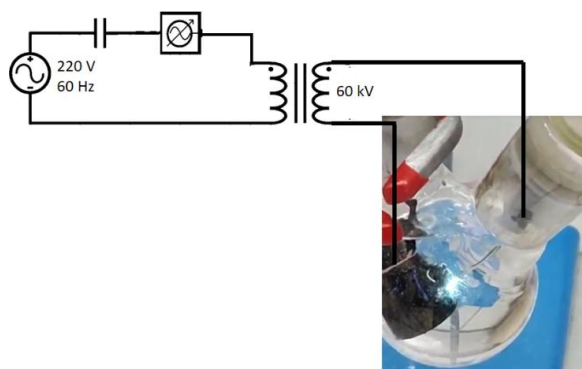
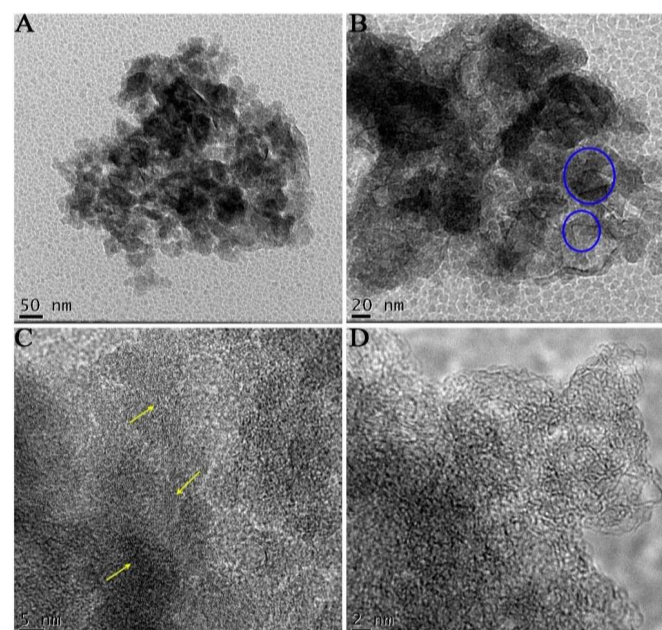


**Figure 1.** Non-thermal plasma generator coupled to a reaction vessel with cyclohexane for graphene production.

The dry material was characterized by transmission electron microscopy (TEM) using a JEOL JEM-2100 electron microscope operated at 200 kV. The material obtained was characterized using scanning electron microscopy (SEM) Jeol JSM-6701F. X-ray diffraction (XRD) was undertaken using a diffractometer model Miniflex II, with a Cu  $k\alpha$  radiation source of 0.15406 Å, set at a  $2\theta$  range of 2–90°, with 2 min<sup>−1</sup> scan speed. The Raman spectra were collected using a Horiba Scientific MacroRam Raman spectroscopy equipment with a laser at 785 nm. Atomic force microscopy was used to observe the graphene deposit on the glass fibers and was carried out in a Multimode 8 using Peak Force Tapping mode and a ScanAsyst-Air probe (resonant frequency ~ 70 kHz, spring constant ~ 0.4 N/m), both from Bruker, under ambient conditions.

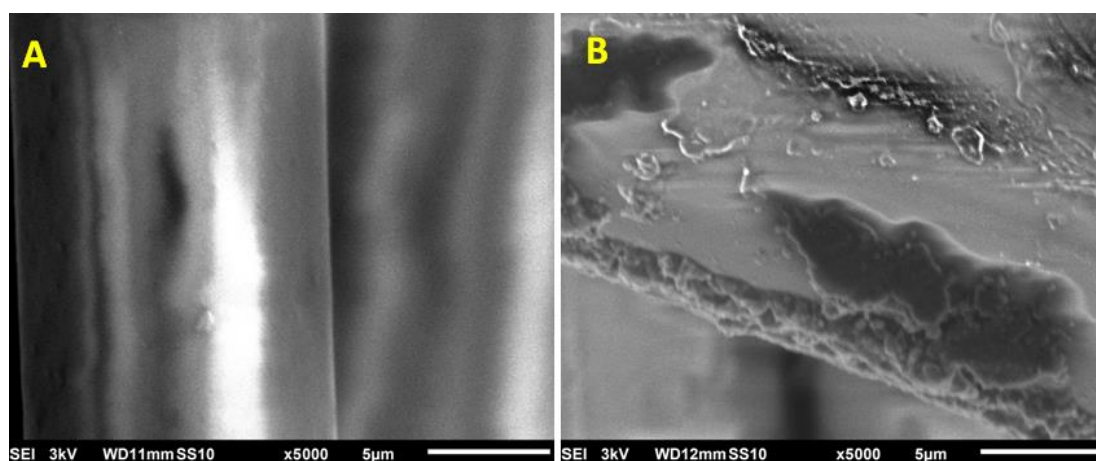
### 3. Results and Discussion

Figure 2 presents TEM images of graphene unsupported nanoflakes (GUN) obtained through non-thermal plasma with cyclohexane. In Figure 2A, agglomerates of particles can be observed, with the transparent regions indicating ultra-thin nanoflakes measuring a few nanometers in size. Furthermore, slightly wrinkled regions are evident, contributing to the distinctive characteristics of graphene [8,9]. Moreover, the morphology of these nanoflakes, which are partially flat, along with regions exhibiting a low level of contrast, suggests a thin graphene layer thickness. However, the occurrence of disordered graphene flakes is also observed. Figure 2B shows regions where the graphene nanoflakes were folded and, in some instances, curled edges were also observed. The layered structure of these nanoflakes is shown in Figure 2C, where there are stacks of about five or more layers. Due to the high resolution of the TEM image (Figure 2D), it is possible to state that the graphene nanostructure is not perfectly flat. It has a partially wrinkled surface that can be designated by regions with different levels of transparency, as discussed above. These nanostructural features provide graphene flakes with promising electronic properties because regions with different levels of transparency or wrinkles create localized energy levels within the band structure, leading to unique electronic states and tunable electronic properties. These states can significantly influence the electronic conductivity and chemical reactivity of graphene [13,14].



**Figure 2.** Transmission electron microscopy of the graphene nanoflakes. (A) Agglomerate nanoparticles at 50 nm; (B) regions that indicate where bent graphene nanoparticles and curled edges are present (blue circles); HRTEM in (C) stacking graphene layers at 5 nm (yellow arrows) and (D) graphene nanostructure details at 2 nm.

SEM images (Figure 3) reveal the smooth and shiny appearance of the fiberglass, similar to what has been reported by other authors in the literature [15,16]. However, after subjecting the fiberglass to the graphene deposition process using non-thermal plasma, referred to in the text as a graphene nanoflake/fiberglass (GN/Fiberglass), clear encrustations of carbonaceous material can be observed on the previously smooth surface. Additionally, surface roughness and defects are noticeable, likely caused by the exfoliation process facilitated by this synthesis setup [12].



**Figure 3.** SEM images of (A) clean fiberglass and (B) GN/Fiberglass.

Figure 4 presents the X-ray diffraction (XRD) analysis of the fiberglass, revealing peaks at  $2\theta = 18.8$  and  $28.9^\circ$  corresponding to silicon oxides (JCPDF 38-360). For the GUN, the diffraction pattern provides evidence of nanoflake stacking and crystallite size within the graphene plane. This evidence can be observed from the (002) and (100) planes, which further corroborates the data obtained from TEM analysis. The presence of a broad peak at  $2\theta = 24.62^\circ$  may suggest a structure with a lower degree of crystallinity. Moreover, the data indicate a degree of amorphism of approximately 48%, where the partially disordered structure exhibits a d-spacing of approximately 0.358 nm between graphene layers. Additionally, the presence of defects affirms the existence of regions in the graphene sheets with increased folding and edge areas, as observed in the TEM images. The peak corresponding to the crystallographic plane (100) presents a d-spacing of 0.208 nm for graphene; this observation suggests the formation of few-layer graphene (FLG) [17]. In the material with graphene nanoflakes on a fiberglass surface (GN/Fiberglass), it was noted that the peaks related to carbon phases are shifted by approximately  $1^\circ$  towards a less positive  $2\theta$  angle, with a d-spacing of 0.2134 for the (100) plane. This indicates an increase in the spacing between graphene layers. Furthermore, there is a degree of amorphism of approximately 55%, where the partially disordered structure exhibits a d-spacing of approximately 0.364 nm between graphene layers.

The Raman spectroscopy analysis provides us with related information, such as the quality of graphene, based on the detailed position, width, shape, and relative amplitude of the peaks. It can also corroborate the TEM and XRD analyses discussed so far. In the Raman spectrum of fiberglass (Figure 5), one can observe the bands at  $1149$ ,  $1625$ , and  $1691\text{ cm}^{-1}$ , which are related to silicon bonded to aluminum, oxygen, and hydrogen [18–20]. Additionally, the bands at  $1385$ ,  $1527$ ,  $1763$ ,  $1847$ , and  $1930\text{ cm}^{-1}$  correspond to boron bonded to hydrogen, boron, and oxygen [21–24]. In the spectrum obtained from GUN, it is possible to observe the three characteristic peaks of graphene: the D, G, and 2D bands centered at approximately  $1320$ ,  $1585$ , and  $2640\text{ cm}^{-1}$ , respectively [25]. The observed peaks in the D and G bands are the result of the convolution of the D1, D2, D3, D4, and G modes in the lower frequency regions of the spectrum at approximately  $1322$ ,  $1623$ ,  $1495$ ,  $1196$ , and  $1587\text{ cm}^{-1}$  [26].

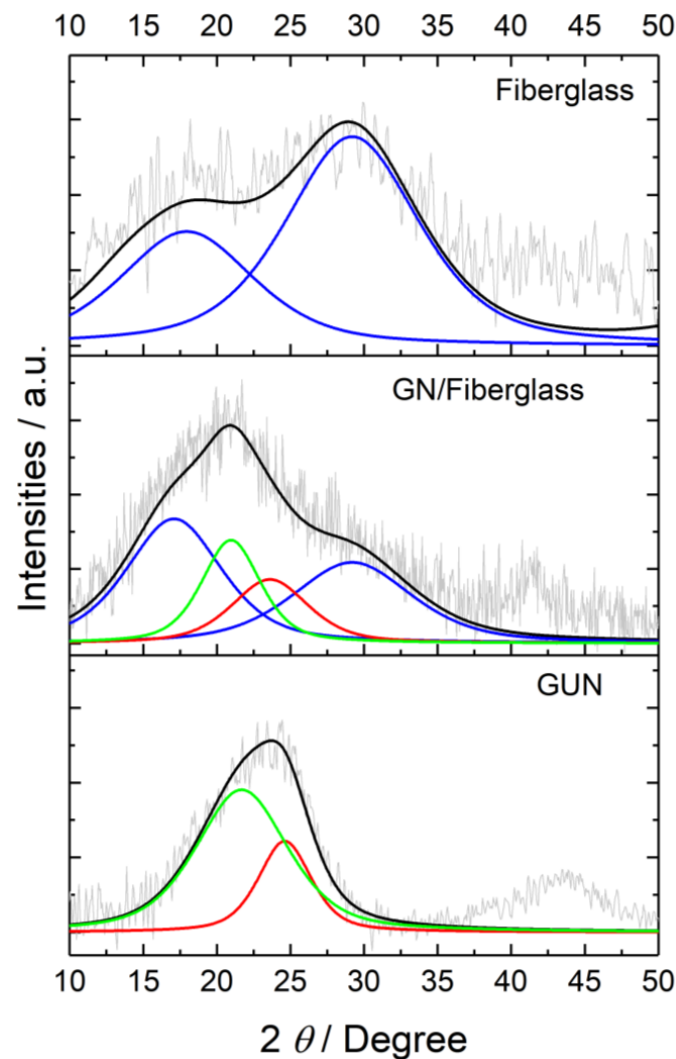


**Figure 4.** X-ray diffraction pattern of fiberglass, GN/Fiberglass, and graphene nanoflakes (GUN) with deconvolution in pseudo-Voigt line forms of the peak corresponding to the (002) plane. Gray for the measured diffractogram, black for the modeled diffractogram, blue for the silicon oxide peaks, green and red for plans referring to carbon phases.

For the GN/Fiberglass material, where the convoluted bands of fiberglass interfere with the resolution of the D and G bands of graphene due to the small amount of material deposited on the fiber, the D2 band of graphene is suppressed. This suppression is likely due to the low-intensity nature of the D2 band, which occurs when a small quantity of material dopes the fiberglass; this is also an indication that the nanoflake was incorporated into the fiberglass.

The literature extensively discusses that the G band corresponds to first-order scattering of  $E_{2g}$  mode, which is related to  $sp^2$  carbon. Additionally, the D band can be attributed to structural defects such as carbon amorphism or edge defects that can affect symmetry and selection rules [27]. The G band is characterized by the number of layers as it reflects the contribution of vibration modes from more carbon atoms. Its intensity, shape, and position provide indications of induced deformations. In the literature, the Raman intensity ratio of the D band to the G band ( $I_D/I_G$ ) is a critical parameter for characterizing the degree of disorder in graphene [25]. In both cases, characteristics of graphene nanoflakes were observed with a ratio of 1.36 for GUN and approximately 3 for GN/Fiberglass, indicating an increase in defects and doping of the carbon structure by components of fiberglass. This

is entirely possible considering the energy employed in the synthesis method, which is capable of exfoliating crystalline structures such as NB [12].

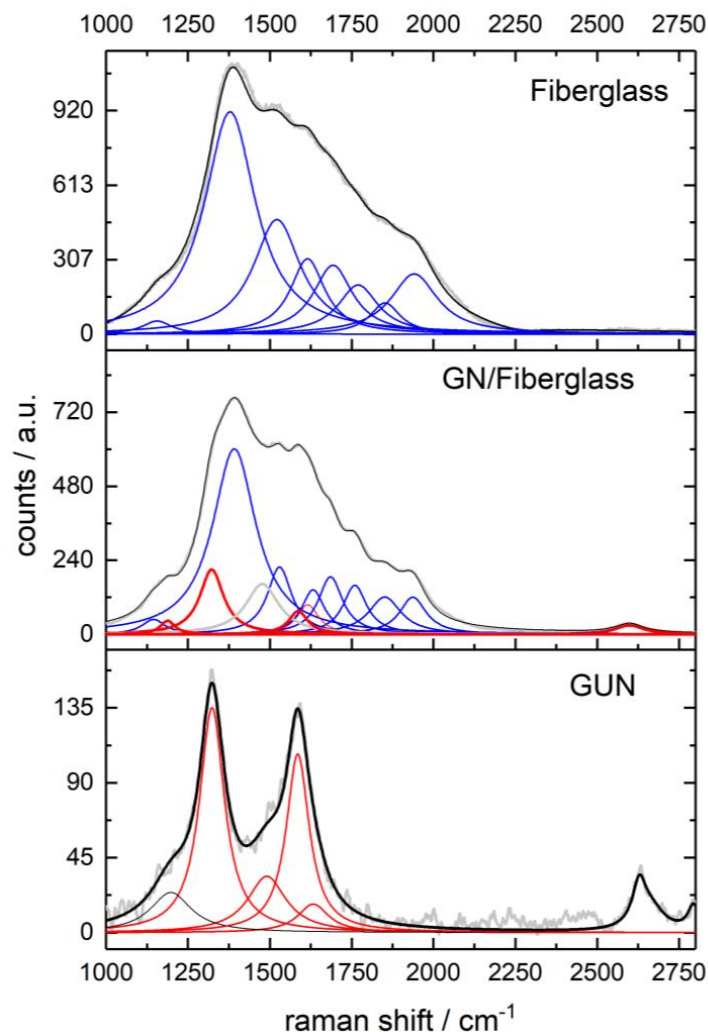


**Figure 5.** Raman spectrum of fiberglass and graphene materials with D, G, and 2D bands and deconvolution of D1, D2, D3, D4, and G bands in lower frequency regions. Light gray for the measured spectrum, black and grey for the modeled spectrum, blue for glass fiber peaks, and red for graphene.

However, the 2D band positioned at  $2631.4\text{ cm}^{-1}$  may indicate the presence of randomly arranged and disordered graphene sheets, as discussed earlier in TEM analyses [17]. The literature indicates that defects observed in the graphene nanostructure may be caused by high anisotropy of mechanical strength or electrical conductivity between in-plane and out-of-plane directions, which can improve material performance for electronics and catalysis applications [28].

Furthermore, the 2D peak may indicate a folded graphene structure, as observed in TEM and XRD data. This effect may be the result of the accumulation of amorphous carbon during material formation [29]. The non-hexagonal defects observed in the discussed graphene nanostructure can increase the reactivity of the basic planes, making these materials active and efficient in heterogeneous catalysis [28].

Figures 6 and 7 illustrate the fiberglass and the graphene nanoflakes deposited on fiberglass by AFM to support the understanding of the fiberglass surface and the formation of graphene layers on it at the nanometric scale. The clean fiberglass has a slight curvature and an irregular surface, as shown in Figure 6A,B, which could not be observed in SEM

(Figure 3A). For a more detailed visualization of the surface irregularities present on it, Figure 6A was flattened prior to the section analysis (Figure 6C), and the corresponding profile can be observed (Figure 6D), with peaks around 30 nm and regions reaching 70 nm in height.

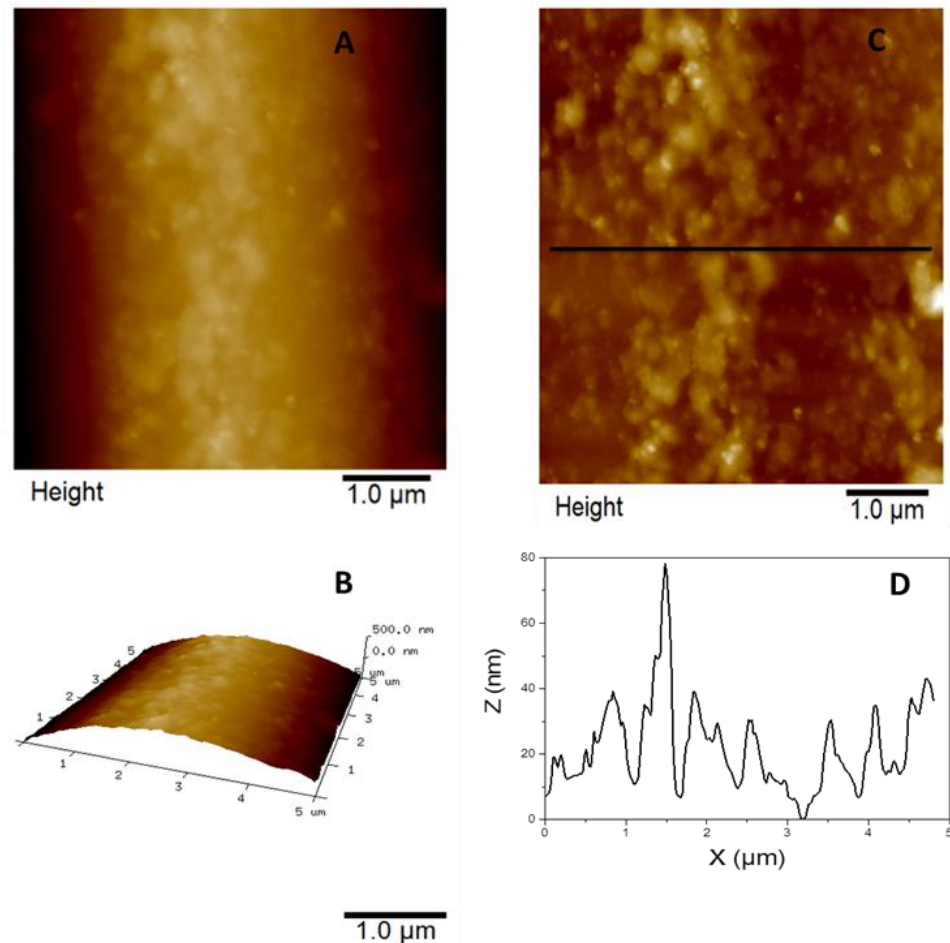


**Figure 6.** Topographic image (A), 3D view (B), flattened image (C), and corresponding profile of the line drawn in (C), (D) of the uncoated fiberglass analyzed by AFM.

Figure 7A presents a topographic AFM image of graphene deposition on fiberglass, where it is possible to see a regular and smooth surface, the layer border shape, and how they are stacked in multilayers (Figure 7A,B). The line profile from Figure 7A is represented in Figure 7C, and it is on the same “Z” scale as Figure 6C for better visualization and comparison. In a smaller scan size (Figure 7D), a step can be seen in detail, and a vertical distance of around 5.7 nm was measured (Figure 7E).

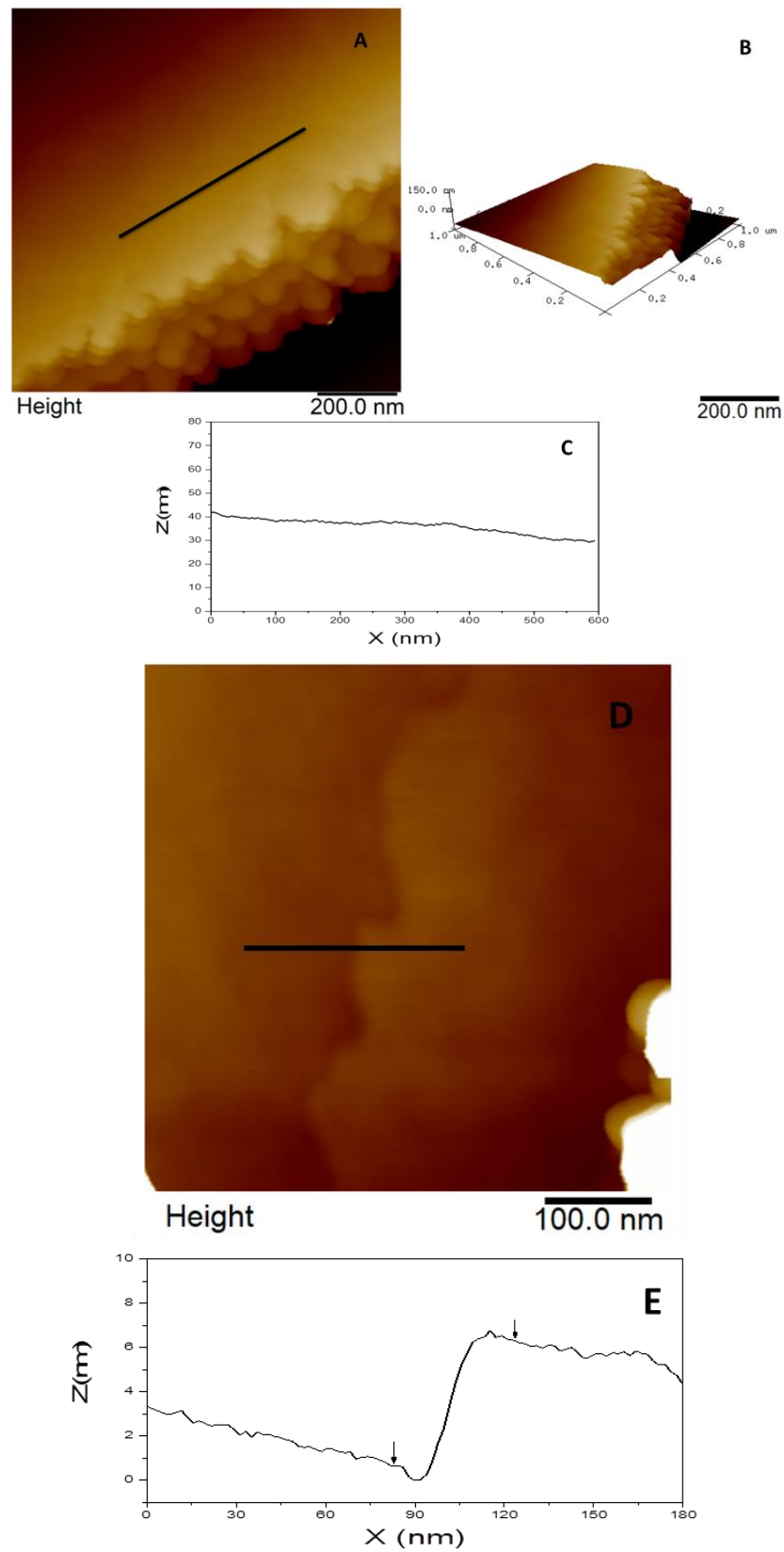


**Figure 7.** Topographic image with a scan size of 1 μm (A), 3D view (B), and corresponding profile of the line drawn in (A,C); topographic image with a scan size of 500 nm (D) and the corresponding profile of the line drawn in (D) and the arrows indicate the position used to calculate the step height (E) of the graphene deposition on a fiberglass analyzed by AFM.



#### 4. Conclusions

The non-thermal plasma setup used to convert cyclohexane into graphene nanoflakes, both supported on fiberglass and unsupported, through a bottom-up approach in a single step, enables rapid synthesis of a nanomaterial with a partially wrinkled and semi-crystalline morphology. The presence of transparent ultrathin layers with a partially disordered structure, exhibiting a d-spacing of 0.358 nm in graphene layers with vacancies, confirms the formation and stacking of few-layered graphene. These properties bestow the material with heterocatalytic efficiency, making it promising for thin film production. X-ray diffraction, Raman spectroscopy, transmission electron microscopy, and atomic force microscopy (AFM) analyses verify the successful deposition of graphene on the glass fibers. The technique developed in this study demonstrates the potential for surface coating without the need for additives, polymers, or solvents. Furthermore, it holds promise for materials studies in various fields, including surface coating and corrosion. This research contributes to the advancement of graphene-based materials and their potential impact in diverse fields.

**Author Contributions:** Conceptualization, A.O.N. and R.F.B.d.S.; methodology, P.V.R.G. and R.N.B.; Microscopies B.P.G.S., J.C.F. and L.O.; writing—original draft preparation, R.N.B., D.R.R.L., R.F.B.d.S. and A.O.N.; supervision, A.O.N.; project administration, D.R.R.L. All authors have read and agreed to the published version of the manuscript.

**Funding:** We are grateful to CAPES, CNPq (350514/2023-2, 302709/2020-7), COPDE/IPEN (2020.06. IPEN.05, 2020.06.IPEN.22.PD), and FAPESP (2017/11937-4) for financial support.

**Institutional Review Board Statement:** Not applicable.

**Informed Consent Statement:** Not applicable.

**Data Availability Statement:** Data can be requested from the authors.

**Conflicts of Interest:** There are no conflict of interest.

#### References

1. Antonova, I.V.; Shavelkina, M.B.; Ivanov, A.I.; Soots, R.A.; Ivanov, P.P.; Bocharov, A.N. Graphene Flakes for Electronic Applications: DC Plasma Jet-Assisted Synthesis. *Nanomaterials* **2020**, *10*, 2050. [[CrossRef](#)] [[PubMed](#)]
2. Zhu, Y.; Qu, B.; Andreeva, D.V.; Ye, C.; Novoselov, K.S. Graphene standardization: The lesson from the East. *Mater. Today* **2021**, *47*, 9–15. [[CrossRef](#)]
3. Dato, A. Graphene synthesized in atmospheric plasmas—A review. *J. Mater. Res.* **2019**, *34*, 214–230. [[CrossRef](#)]
4. Paton, K.R.; Varrla, E.; Backes, C.; Smith, R.J.; Khan, U.; O'Neill, A.; Boland, C.; Lotya, M.; Istrate, O.M.; King, P.; et al. Scalable production of large quantities of defect-free few-layer graphene by shear exfoliation in liquids. *Nat. Mater.* **2014**, *13*, 624–630. [[CrossRef](#)] [[PubMed](#)]
5. Chu, J.; Marsden, A.J.; Young, R.J.; Bissett, M.A. Graphene-Based Materials as Strain Sensors in Glass Fiber/Epoxy Model Composites. *ACS Appl. Mater. Interfaces* **2019**, *11*, 31338–31345. [[CrossRef](#)]
6. Hadden, C.M.; Klimek-McDonald, D.R.; Pineda, E.J.; King, J.A.; Reichenadter, A.M.; Miskioglu, I.; Gowtham, S.; Odegard, G.M. Mechanical properties of graphene nanoplatelet/carbon fiber/epoxy hybrid composites: Multiscale modeling and experiments. *Carbon* **2015**, *95*, 100–112. [[CrossRef](#)]
7. Fang, M.; Xiong, X.; Hao, Y.; Zhang, T.; Wang, H.; Cheng, H.-M.; Zeng, Y. Preparation of highly conductive graphene-coated glass fibers by sol-gel and dip-coating method. *J. Mater. Sci. Technol.* **2019**, *35*, 1989–1995. [[CrossRef](#)]
8. Ismail, A.; Zubaydi, A.; Piscesa, B.; Tuswan, T. A novel fiberglass-reinforced polyurethane elastomer as the core sandwich material of the ship-plate system. *J. Mech. Behav. Mater.* **2023**, *32*, 20220288. [[CrossRef](#)]
9. Groo, L.; Nasser, J.; Zhang, L.; Steinke, K.; Inman, D.; Sodano, H. Laser induced graphene in fiberglass-reinforced composites for strain and damage sensing. *Compos. Sci. Technol.* **2020**, *199*, 108367. [[CrossRef](#)]
10. Gupta, S.; Joshi, P.; Narayan, J. Electron mobility modulation in graphene oxide by controlling carbon melt lifetime. *Carbon* **2020**, *170*, 327–337. [[CrossRef](#)]
11. Shavelkina, M.B.; Filimonova, E.A.; Amirov, R.K. Effect of helium/propane-butane atmosphere on the synthesis of graphene in plasma jet system. *Plasma Sources Sci. Technol.* **2020**, *29*, 025024. [[CrossRef](#)]
12. De Souza, R.F.B.; Maia, V.A.; Zambiazzi, P.J.; Otubo, L.; Lazar, D.R.R.; Neto, A.O. Facile, clean and rapid exfoliation of boron-nitride using a non-thermal plasma process. *Mater. Today Adv.* **2021**, *12*, 100181. [[CrossRef](#)]
13. Zhang, X.; Li, K.; Li, H.; Lu, J.; Fu, Q.; Chu, Y. Graphene nanosheets synthesis via chemical reduction of graphene oxide using sodium acetate trihydrate solution. *Synth. Met.* **2014**, *193*, 132–138. [[CrossRef](#)]

14. Pimenta, M.A.; Dresselhaus, G.; Dresselhaus, M.S.; Cançado, L.G.; Jorio, A.; Saito, R. Studying disorder in graphite-based systems by Raman spectroscopy. *Phys. Chem. Chem. Phys.* **2007**, *9*, 1276–1290. [[CrossRef](#)]
15. Vitorino, L.S.; Oréface, R.L. Layer-by-Layer technique employed to construct multitask interfaces in polymer composites. *Polímeros* **2017**, *27*, 330–338. [[CrossRef](#)]
16. Matrenichev, V.; Belone, M.C.L.; Palola, S.; Laurikainen, P.; Sarlin, E. Resizing Approach to Increase the Viability of Recycled Fibre-Reinforced Composites. *Materials* **2020**, *13*, 5773. [[CrossRef](#)] [[PubMed](#)]
17. Wu, Y.; Wang, B.; Ma, Y.; Huang, Y.; Li, N.; Zhang, F.; Chen, Y. Efficient and large-scale synthesis of few-layered graphene using an arc-discharge method and conductivity studies of the resulting films. *Nano Res.* **2010**, *3*, 661–669. [[CrossRef](#)]
18. Zhu, Q.; Wang, H.; Tian, Y.; Gao, R.; Zhao, S.; Huang, L.; Xu, S.; Zhang, X. The forming region and mechanical properties of CaO-Al<sub>2</sub>O<sub>3</sub>-SiO<sub>2</sub> system. *Ceram. Int.* **2017**, *43*, 13810–13816. [[CrossRef](#)]
19. McMillan, P.F.; Poe, B.T.; Stanton, T.R.; Remmele, R.L. A Raman spectroscopic study of H/D isotopically substituted hydrous aluminosilicate glasses. *Phys. Chem. Miner.* **1993**, *19*, 454–459. [[CrossRef](#)]
20. Potts, A.W.; Price, W.C. The photoelectron spectra of methane, silane, germane and stannane. *Proc. R. Soc. Lond. A* **1997**, *326*, 165–179. [[CrossRef](#)]
21. Akagi, R.; Ohtori, N.; Umesaki, N. Raman spectra of K<sub>2</sub>O-B<sub>2</sub>O<sub>3</sub> glasses and melts. *J. Non-Cryst. Solids* **2001**, *293–295*, 471–476. [[CrossRef](#)]
22. Yano, T.; Kunimine, N.; Shibata, S.; Yamane, M. Structural investigation of sodium borate glasses and melts by Raman spectroscopy: I. Quantitative evaluation of structural units. *J. Non-Cryst. Solids* **2003**, *321*, 137–146. [[CrossRef](#)]
23. Webb, A.N.; Neu, J.T.; Pitzer, K.S. The Infra-Red and Raman Spectra and the Thermodynamic Properties of Diborane. *J. Chem. Phys.* **2004**, *17*, 1007–1011. [[CrossRef](#)]
24. Burkholder, T.R.; Andrews, L. Reactions of boron atoms with molecular oxygen. Infrared spectra of BO, BO<sub>2</sub>, B<sub>2</sub>O<sub>2</sub>, B<sub>2</sub>O<sub>3</sub>, and BO<sub>2</sub><sup>-</sup> in solid argon. *J. Chem. Phys.* **1991**, *95*, 8697–8709. [[CrossRef](#)]
25. Ferrari, A.C.; Basko, D.M. Raman spectroscopy as a versatile tool for studying the properties of graphene. *Nat. Nanotechnol.* **2013**, *8*, 235–246. [[CrossRef](#)]
26. Lu, Z.; Wang, C.; Chen, X.; Song, M.; Xia, W. Effects of buffer gas on N-doped graphene in a non-thermal plasma process. *Diam. Relat. Mater.* **2021**, *118*, 108548. [[CrossRef](#)]
27. Wu, J.-B.; Lin, M.-L.; Cong, X.; Liu, H.-N.; Tan, P.-H. Raman spectroscopy of graphene-based materials and its applications in related devices. *Chem. Soc. Rev.* **2018**, *47*, 1822–1873. [[CrossRef](#)] [[PubMed](#)]
28. Zhang, L.-H.; Yu, F.; Shiju, N.R. Carbon-Based Catalysts for Selective Electrochemical Nitrogen-to-Ammonia Conversion. *ACS Sustain. Chem. Eng.* **2021**, *9*, 7687–7703. [[CrossRef](#)]
29. Hao, Y.; Wang, Y.; Wang, L.; Ni, Z.; Wang, Z.; Wang, R.; Koo, C.K.; Shen, Z.; Thong, J.T.L. Probing Layer Number and Stacking Order of Few-Layer Graphene by Raman Spectroscopy. *Small* **2010**, *6*, 195–200. [[CrossRef](#)]

**Disclaimer/Publisher’s Note:** The statements, opinions and data contained in all publications are solely those of the individual author(s) and contributor(s) and not of MDPI and/or the editor(s). MDPI and/or the editor(s) disclaim responsibility for any injury to people or property resulting from any ideas, methods, instructions or products referred to in the content.